

Seismic performance evaluation of moment frames with slit-friction hybrid dampers

Joonho Lee and Jinkoo Kim*

*Department of Civil and Architectural Engineering, Sungkyunkwan University,
Cheoncheon-dong, Suwon, Korea*

(Received July 4, 2014, Revised July 7, 2015, Accepted July 21, 2015)

Abstract. This study investigates the seismic energy dissipation capacity of a hybrid passive damper composed of a friction and a hysteretic slit damper. The capacity of the hybrid device required to satisfy a given target performance of a reinforced concrete moment resisting frame designed with reduced design base shear is determined based on the ASCE/SEI 7-10 process, and the seismic performances of the structures designed without and with the hybrid dampers are verified by nonlinear dynamic analyses. Fragility analysis is carried out to investigate the probability of a specified limit state to be reached. The analysis results show that in the structure with hybrid dampers the residual displacements are generally reduced and the dissipated inelastic energy is mostly concentrated on the dampers. At the Moderate to Extensive damage states the fragility turned out to be smallest in the structure with the hybrid dampers.

Keywords: hybrid dampers; slit dampers; friction dampers; seismic performance; fragility analysis

1. Introduction

Recently various seismic energy dissipation devices have been applied to enhance seismic safety of building structures. Typical energy dissipation devices include friction devices, metallic yield devices, viscous dampers, etc. The seismic performances of hysteretic passive energy dissipative devices have been investigated such as ADAS device (Bergman and Goel 1987), slit dampers (Chan and Albermani 2008, Oh *et al.* 2009), friction dampers (Lee *et al.* 2008, Kim *et al.* 2011, Patel and Jangid 2011), and buckling restrained braces (Choi and Kim 2006, Kim *et al.* 2009). Tremblay *et al.* (2014) carried out comparative study of tied braced frames with three types of energy dissipation devices such as friction dampers, buckling restrained bracing members, and self-centering energy dissipative devices. Some researchers investigated simultaneous application of multiple devices to maximize the energy dissipation mechanism. Tsai *et al.* (1998) and Chen *et al.* (2002) combined displacement-dependent and velocity-dependent devices for seismic mitigation of structures to minimize the shortcomings of individual dampers, and proposed the most economical solution for seismic mitigation. Marshall and Charney (2012) studied the concept of the hybrid passive control system with BRB and viscous fluid device by investigating the

*Corresponding author, Professor, E-mail: jkim12@skku.edu

seismic response of steel frame structures. Optimum design procedures were developed for application of hybrid passive dampers. Uetani *et al.* (2003) applied the gradient projection algorithm for optimum design of a real building structure with viscous and hysteretic dampers. Murakami *et al.* (2013) proposed a sensitivity-based practical optimization method for simultaneous use of viscous, hysteretic, and inertial mass dampers for earthquakes.

This study developed a hybrid passive energy dissipation device composed of a friction damper combined with a steel plate slit damper. The hybrid damper has an advantage in that only a friction damper is activated for wind load or small earthquakes, and combined action of a friction damper and a hysteretic damper is induced for strong earthquakes. The residual displacement in the friction dampers caused by strong wind or small earthquakes can be recovered by the structure and the slit dampers which still remain elastic and provide restoring force for the friction dampers. For seismic design and retrofit of a structure, the capacity of the hybrid device to satisfy a given target performance was determined based on the ASCE/SEI 7-10 process. The effect of the device was verified by nonlinear time-history analysis and fragility analysis.

2. Nonlinear modeling of hybrid slit-friction dampers

The steel plate slit damper is composed of many vertical strips as shown in Fig. 1. The in-plane stiffness of the slit damper subjected to horizontal shear force can be obtained as follows based on the assumption that the ends of the narrow strips are fully restrained from rotation

$$k_d = n \frac{12EI}{l_o^3} = n \frac{Etb^3}{l_o^3} \quad (1)$$

where n =number of strips, t =thickness of strips, b =width of strips, and l_o =length of the vertical strip. Chan and Albermani (2008) derived the yield strength of a slit damper assuming elastic-perfectly-plastic behavior, which is summarized as follows. When displacement is large, plastic hinges form at both ends of the strip with the full plastic moment M_p obtained by multiplication of the yield stress and the plastic section modulus

$$M_p = \sigma_y \frac{tb^2}{4} \quad (2)$$

From the equivalence of the internal work, $P_y \delta_p$, and the external work, $2nM_p \theta_p$, where δ_p is the plastic displacement, $l_o \theta_p$, and θ_p is the plastic rotation, the yield force of the slit damper, P_y , can be obtained as follows

$$P_y = F_{y,slit} = \frac{2nM_p}{l_o} = \frac{n \sigma_y tb^2}{2l_o} \quad (3)$$

The yield stress of the slit damper used in this study is 325 MPa, the thickness of the strip t is 20 mm, the length of the slit l_o is 200 mm, and the number of strip n is 9. The width of the strip b is varied from 15 mm to 20 mm. Using these information the yield strength and yield displacement of the slit damper are listed in Table 1.

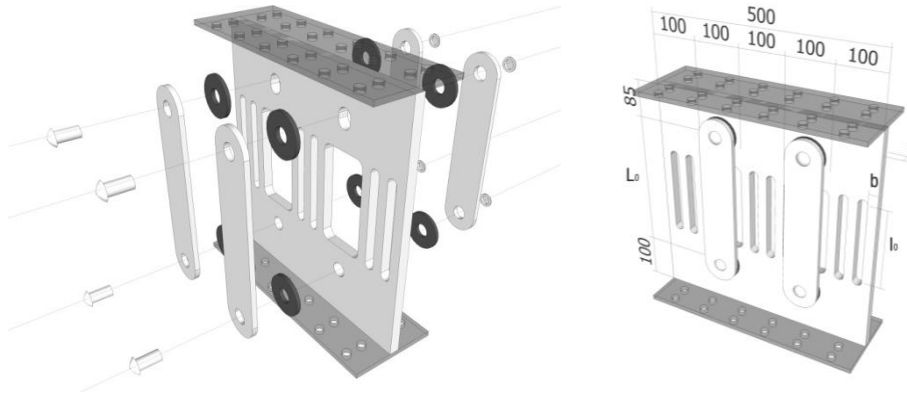


Fig. 1 Configuration of a hybrid slit-friction damper

Table 1 Types of steel slit dampers used in the analysis

ID	σ_y (N/mm ²)	t (mm)	n	b (mm)	l_0 (mm)	b/l_0	P_y (N)	δ_y (mm)
S1				15.0		0.075	32906	2.1
S2				15.5		0.078	35137	2.0
S3				16.0		0.08	37440	2.0
S4				16.5		0.083	39817	1.9
S5				17.0		0.085	42266	1.8
S6	325	20	9	17.5	200	0.088	44789	1.8
S7				18.0		0.09	47385	1.8
S8				18.5		0.093	50054	1.7
S9				19.0		0.095	52796	1.7
S10				19.5		0.098	55612	1.6
S11				20.0		0.1	58500	1.6

A friction damper is activated when the applied load reaches the slip force. As the initial stiffness of a friction damper is very large, larger energy is dissipated compared with hysteretic dampers with similar yield force. The equilibrium between the lateral force F and the rotational moment at the friction pad M is as follows

$$2M = FL_0 \tag{4}$$

where L_0 is the length between the two slip pads. The rotational moment at the friction pad is obtained from the following equation (DAMPTECH 2014)

$$M = \mu N Q R_m = \mu N Q \left[0.5(R_1^2 + R_2^2) \right]^{1/2} \tag{5}$$

where μ is the friction coefficient of the friction pad, N is the number of friction face, Q is the

clamping force, and R_m is the effective area of the friction face, R_1 and R_2 are the inner and the outer radii of the friction face, respectively. From Eq. (4) and Eq. (5) the yield force of the friction damper can be obtained as follows

$$F_{y, friction} = 2\mu NQ \frac{R_m}{L_0} \tag{6}$$

In this study a couple of friction dampers were used for each hybrid damper, one at each side of the slip damper. The friction coefficient of the friction pad was assumed to be 0.35 based on Blau (2001), and the number of friction face (N) is 2 for each friction damper. The clamping force of the bolt (Q) was varied from 50 to 100 kN. Table 2 summarizes the information of the friction dampers used in the analysis.

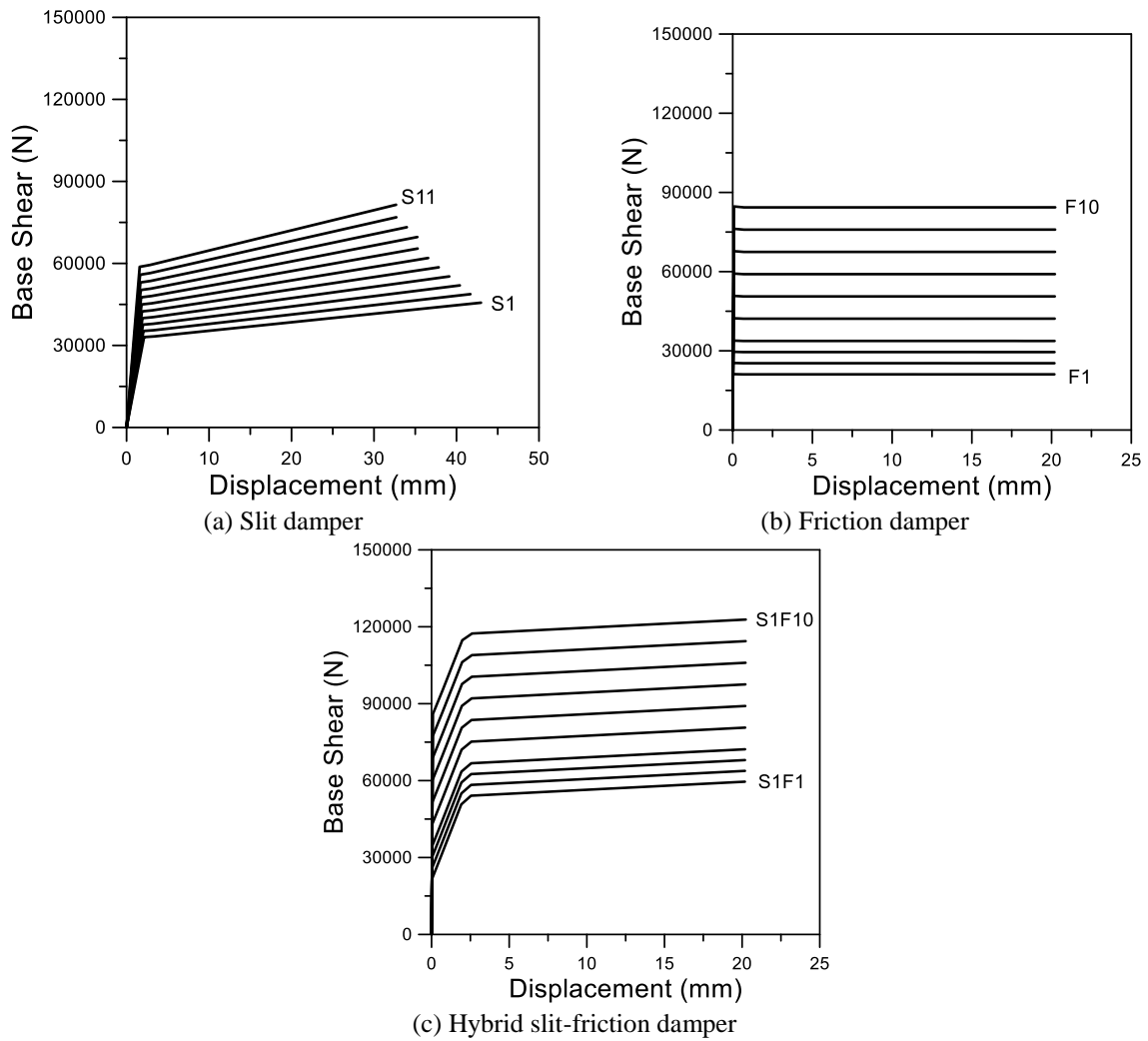


Fig. 2 Nonlinear force-displacement relationships of the dampers

Table 2 Types of friction dampers used in the analysis

ID	μ	N	Q (N)	R_1 (mm)	R_2 (mm)	R_m (mm)	L (mm)	F (N)
F1	0.35	4	50,000	30	60	47.43416	315	21081.85
F2	0.35	4	60,000	30	60	47.43416	315	25298.22
F3	0.35	4	70,000	30	60	47.43416	315	29514.59
F4	0.35	4	80,000	30	60	47.43416	315	33730.96
F5	0.35	8	50,000	30	60	47.43416	315	42163.70
F6	0.35	8	60,000	30	60	47.43416	315	50596.44
F7	0.35	8	70,000	30	60	47.43416	315	59029.18
F8	0.35	8	80,000	30	60	47.43416	315	67461.92
F9	0.35	8	90,000	30	60	47.43416	315	75894.66
F10	0.35	8	100,000	30	60	47.43416	315	84327.40

In case the slit damper and the friction damper are connected in parallel as shown in Fig. 1, the yield strength of the hybrid damper can be obtained as follows

$$F_{y, hybrid} = F_{y, slit} + F_{y, friction} = \left(\frac{n \sigma_y t b^2}{2l_o} \right) + \left(\frac{2 \mu N Q R_m}{L} \right) \quad (7)$$

In this paper the behavior of the hybrid damper was modeled using the ‘Rubber Type Seismic Isolator Element’ provided in the nonlinear analysis code Perform 3D (2006). The post-yield stiffness of the slit damper was assumed to be 2 % of the initial stiffness, and the maximum yield displacement of the friction damper was set to be 20 mm based on the data provided by the DAMPTECH. Fig. 2(a) and 2(b) show the nonlinear static analysis results of the slit and the friction dampers, and Fig. 2(c) represents the pushover curves of the hybrid damper in which a slit damper is combined with two friction dampers. At the slip load the friction damper yielded first, and as the load further increased the slit damper started to yield and deformed inelastically.

3. Design of analysis model structures

3.1 Design of analysis model structures

The prototype analysis model structure is a five-story RC frame structure assumed to be located in downtown Los Angeles. Structural members were designed using ACI 318 (2011), and the design seismic load was determined based on ASCE/SEI 7-10 (2010). The perimeter frames were designed as special moment frames and the internal moment frames were designed as gravity load-resisting frames. Fig. 3 shows the structural plan and the elevation view of the model structure. For gravity loads, the dead and live loads of 7.0 kN/m² and 1.92 kN/m² were used, respectively. The design seismic load was computed based on the design spectral response acceleration parameters $S_{DS}=0.73$ g and $S_{D1}=0.60$ g. This corresponds to the design seismic load in Los Angeles area with site class D. For a RC special moment frame, the response modification

factor (R) and the deflection amplification factor (C_d) specified in the ASCE/SEI 7-10 are 8.0 and 5.5, respectively. Using those design parameters the seismic design base shear was computed as 6793.7 kN. Structural member design of the special moment frames used in the analysis was carried out based on the ‘Special Provisions for Seismic Design’ of ACI 318-11. When the structure was subjected to the design seismic load, the maximum inter-story drift turned out to be 3.6 % of the story height, and the structure was redesigned to satisfy the maximum inter-story drift of 2 %. Table 3 and 4 show the details of the member design.

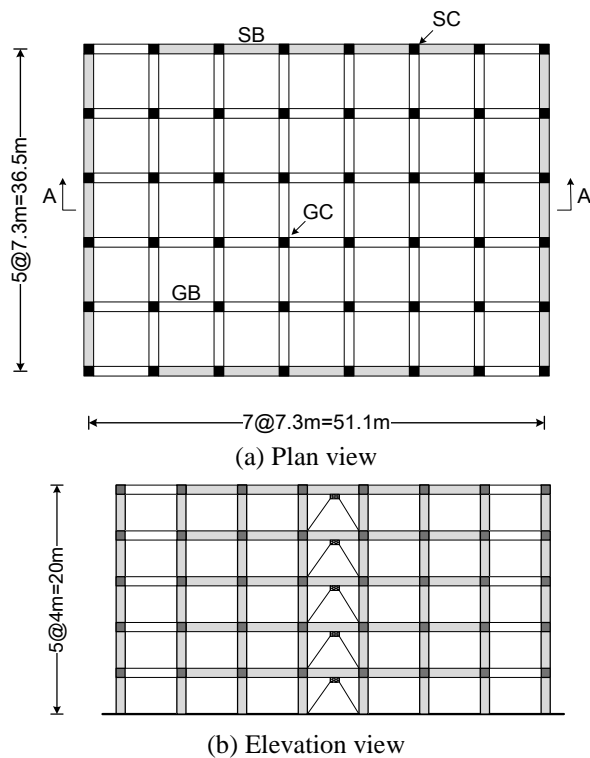


Fig. 3 Configuration of 5-story analysis model structure

Table 3 Section property of beams in prototype structure

Section	Size(mm)	Stirrup		Main rebars			
		Exterior	Interior	Exterior		Interior	
				Top	Bottom	Top	Bottom
GB	460×500	D13@125	D13@400	3-D25	5-D25	3-D25	8-D25
SB1	560×760	D16@100	D16@200	12-D25	9-D25	5-D25	5-D25
SB2	560×740	D16@100	D16@200	14-D25	12-D25	6-D25	6-D25
SB3	560×720	D16@125	D16@200	13-D25	10-D25	5-D25	6-D25
SB4	560×700	D16@125	D16@200	10-D25	8-D25	4-D25	4-D25
SB5	560×680	D16@150	D16@300	6-D25	6-D25	3-D25	3-D25

Table 4 Section property of columns in prototype structure

Section	Size(mm)	Tie bars	Main rebars
GC	500×500	D13@200	12-D25
SC1	760×760	D19@100	16-D32
SC2	760×760	D19@100	16-D32
SC3	760×760	D19@100	16-D32
SC4	720×720	D19@125	16-D29
SC5	720×720	D19@125	16-D29

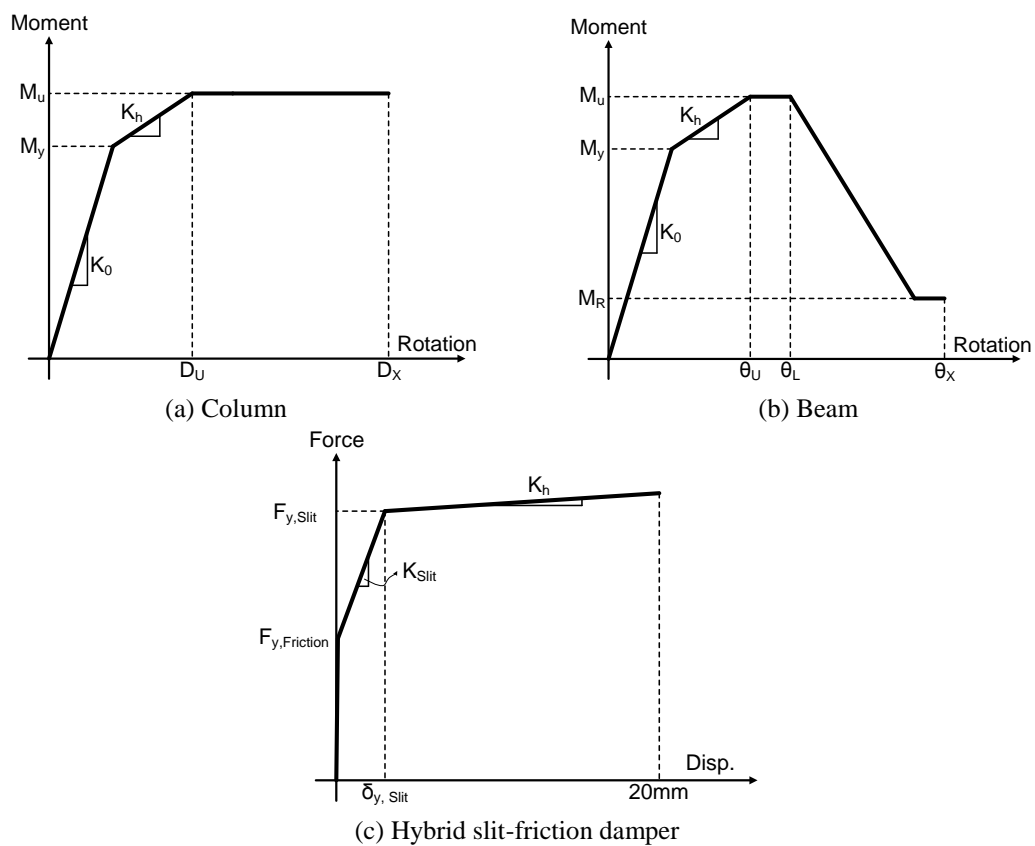


Fig. 4 Nonlinear moment-rotation relationships of structural elements

3.2 Design of a structure with hybrid slit-friction dampers

ASCE/SEI 7-10 specifies nonlinear static and dynamic analyses, response spectrum analysis, and equivalent lateral force procedure for design of a structure with energy dissipation devices. In this study the prototype five-story special moment frame was redesigned using hybrid dampers following the response spectrum analysis procedure of the ASCE/SEI 7-10. The dampers were installed at the center bay of the structure as shown in Fig. 3. The design process of the structure with damping devices is as follows: the effective ductility demand (μ_D) of the seismic force

resisting system is assumed and the effective damping at the design displacement (β_{mD}) of the structure with damping system is computed. Then using Table 18.6-1 of ASCE/SEI 7-10 the numerical coefficient for damped response modification factor corresponding to the β_{mD} is obtained, and the validity of the design base shear and the ductility factor assumed in the beginning of the design stage is verified.

In ASCE/SEI 7-10 the seismic base shear used for design of the structure with dampers is determined as the larger of $\frac{V}{B_{v+l}}$ or $0.75V$, where V is the seismic design base shear and B_{v+l} is the numerical coefficient for effective damping equal to the sum of equivalent viscous damping and inherent damping. In this study the design base shear for the damped structure was reduced to 75% of the design base shear of the prototype structure, which is 5,095 kN. The member properties of the redesigned structure are presented in Tables 5 and 6. Table 7 shows the natural periods and mode shapes of the model structures. The capacity of the hybrid dampers was determined to be 25% of the story shear of the model structure, which was divided into 60% for the slit dampers and 40% for the friction dampers. Table 8 shows the eigenvalue analysis results of the structure with hybrid dampers. The modal properties presented in Tables 7 and 8 were used to construct the idealized elasto-plastic pushover curve shown in Fig. 4. The validity of the design was checked by the ASCE/SEI 7-10 procedure which is described as follows.

The effective ductility ratio of the model structure with hybrid dampers corresponding to the fundamental mode, μ_{1D} , was assumed to be 1.75, and the effective fundamental mode period at the design earthquake ground motion, T_{1D} , was computed to be 2.17 second using the following equation

Table 5 Section property of beams in the damped structure

Section	Size(mm)	Stirrup		Main rebars			
		Exterior (i, j)	Interior (m)	Exterior (i, j)		Interior (m)	
				Top	Bottom	Top	Bottom
GB	460×500	D13@125	D13@400	3-D25	5-D25	3-D25	8-D25
SB1	420×580	D16@125	D16@300	11-D25	8-D25	4-D25	5-D25
SB2	420×560	D16@125	D16@300	14-D25	10-D25	5-D25	5-D25
SB3	420×540	D16@125	D16@300	14-D25	10-D25	5-D25	5-D25
SB4	420×520	D16@125	D16@300	11-D25	7-D25	4-D25	4-D25
SB5	420×500	D16@150	D16@300	8-D25	4-D25	3-D25	3-D25

Table 6 Section property of columns in damped structure

Section	Size(mm)	Tie bars	Main rebars
GC	500×500	D13@200	12-D25
SC1	620×620	D19@100	16-D32
SC2	620×620	D19@100	16-D32
SC3	620×620	D19@100	16-D32
SC4	580×580	D19@125	16-D29
SC5	580×580	D19@125	16-D29

Table 7 Modal properties of the prototype structure

Modes	1st	2nd	3rd
Periods	2.0212	0.5847	0.2672
Mode Shape	5	1	-0.7428
	4	0.8134	-0.1001
	3	0.5816	-0.8819
	2	0.3321	-0.9449
	1	0.1093	-0.4274
Modal Weight, W_m (kN)	66315.5019	12345.1002	5364.5985
Modal participation factor, Γ_m	1.3446	-0.4973	-0.2923

Table 8 Modal properties of the damped structures

Modes	1st	2nd	3rd
Periods	1.0818	0.3645	0.1959
Mode Shape	5	1.0818	1
	4	1	-0.1103
	3	0.8024	-0.8407
	2	0.5779	-0.9212
	1	0.3469	-0.4608
Modal Weight, W_m (kN)	0.1291	12542.9679	4446.5787
Modal participation factor, Γ_m	67740.1101	-0.5042	-0.2773

$$T_{1D} = T_1 \sqrt{\mu_D} \tag{8}$$

where T_1 is the fundamental period of the structure. In ASCE/SEI 7-10 the design spectrum can be reduced using the effective damping modification factor B_{1D} . The effective damping of the structure with dampers consists of the inherent damping (ζ_I) of 5% of the critical damping, hysteretic damping ($\zeta_{HD,f}$) due to inelastic deformation of the structural elements, and the damping from the damping devices ($\zeta_{HD,d}$) which is obtained from the following equation

$$\zeta_{HD,f} = q_H (0.64 - \zeta_I) \left(1 - \frac{I}{\mu_f} \right) \tag{9}$$

$$q_H = 0.67 \frac{S_{D1}/S_{DS}}{T_1} \tag{10}$$

where q_H is the hysteresis loop adjustment factor considering the reduction of hysteresis curve due to pinching. The effective damping ratio of the 5-story model structure turned out to be 0.19 and the corresponding damping coefficient B_{1D} be 1.48. The design base shear of the structure which allows inelastic behavior was obtained using the following code formula

Table 9 Important points on the idealized force displacement curve of the damped structure

Point	Base shear (kN)	Roof disp. (mm)
1	1701.15	6.444
2	2805.74	6.444
3	3182.91	65.580
4	4884.05	65.580
5	12210.13	136.95

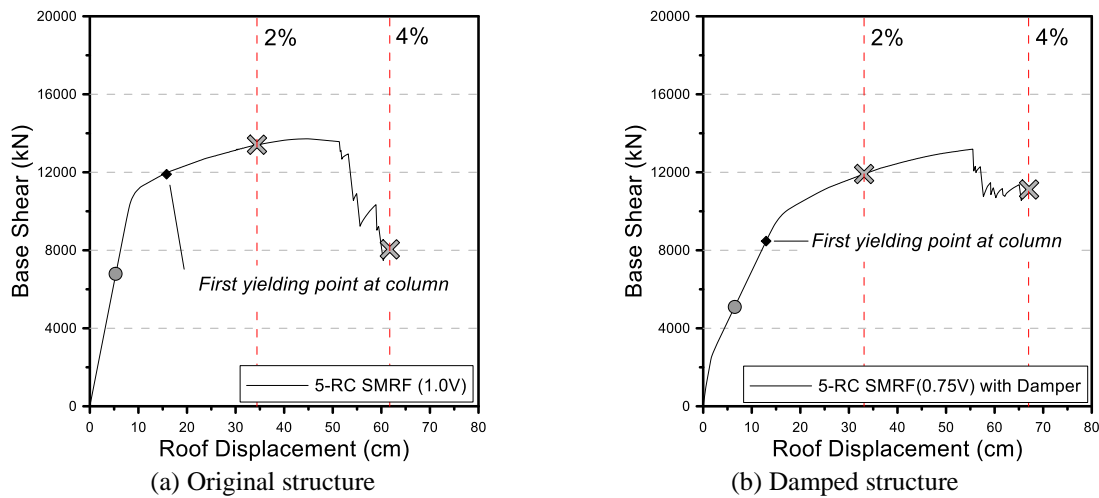


Fig. 5 Pushover analysis results of the 5-story analysis model structures

$$V_{ID} = \frac{R}{C_d \Omega_o} \frac{S_a}{B_{ID}} W_{ID} = \frac{R}{C_d \Omega_o} \frac{S_{DI}}{T_{ID} B_{ID}} W_{ID} \quad (11)$$

where T_{ID} is the effective period of the fundamental mode of the structure at the design displacement in the direction under consideration, and W_{ID} is the effective modal weight. Using the design base shear, the yield strength of the model structure was obtained as follows

$$V_Y = \frac{C_d \Omega_o}{R} V_{ID} \quad (12)$$

Using the above equation the yield strength of the model structure with hybrid dampers was computed as 12.21 MN, which is close to point 5 of Table 9. The ductility ratio of the damped structure, μ_D , was obtained as 1.80 from the ratio of the first mode roof displacement, D_{1D} , and the yield displacement at the roof, D_Y . This value is similar to the assumed first mode effective ductility, μ_{1D} , which is 1.75, and is less than the allowable maximum ductility of 2.67. This implies that the assumed seismic design base shear in the beginning of the design process is acceptable.

4. Seismic performance evaluation of model structures

4.1 Properties of analysis models

Non-linear analyses of the model structures were carried out using the program code Perform-3D (2006). The moment-rotation relationships of the columns and beams were modeled using the 'FEMA column and beam, concrete type' elements provided in the Perform-3D, which are illustrated in Fig. 4(a) and 4(b), respectively. The force-displacement relationship of the hybrid slit dampers is illustrated in Fig. 4(c). The ultimate strength of concrete is 27 MPa and the tensile strength of re-bars is 400 MPa. The damping ratio was assumed to be 5% of the critical damping in all vibration modes.

4.2 Nonlinear static analysis results

To evaluate overall strength and failure mode of model structures, nonlinear static pushover analyses were carried out using the program code Perform 3D (2006). The lateral load pattern was determined to be proportional to the fundamental mode shape of the model structures. Fig. 5(a) and 5(b) depict the pushover curves of the model structure designed without dampers (prototype structure) and the structure designed using 75% of the design base shear plus hybrid dampers, respectively. It can be observed that, as expected, the structure with dampers showed smaller initial stiffness than the structure without dampers. In the structure with dampers the first plastic hinge formed in the first story columns at the smaller load. Even though the strength of the prototype structure at the maximum inter-story drift of 2% of the story height is slightly higher than that of the damped structure, the opposite is true in the strengths at the maximum inter-story drift of 4% of the story height. Even though the damped structure was designed with only 75% of the design base shear of the prototype structure, the maximum strengths of the prototype and the damped structure are quite close to each other.

Fig. 6 depicts the plastic hinge formation in the analysis model structures at the maximum inter-story drift of 2% of the story height. As the original structure without the dampers was designed to meet the weak beam - strong column requirement of ACI 318 code, plastic hinges first formed at the beams and were subsequently spread to the first story columns. In the structure with hybrid slit-friction dampers the formation of the plastic hinges is similar to that of the original structure except that no plastic hinge was observed in the second story beams and plastic hinges formed in the first story columns only at the center bay where the damper was installed. It was observed that in both model structures the rotations of the plastic hinges were within the IO (Immediate Occupancy) limit state specified in the ASCE/SEI 41-06.

Table 10 Earthquake records used in the dynamic analysis

	Name	Component	PGA Max. (g)
1C1	Northridge	NORTHR/MUL009	0.52
5C1	Imperial Valley	IMPVALL/H-DLT262	0.35
7C1	Kobe	KOBE/MIS000	0.51
13C1	Loma Prieta	LOMAP/CAP000	0.53
16C1	Superstition Hills	SUPERST/B-ICC000	0.36
19C1	Chi-Chi	CHICHI/CHY101-E	0.44
21C1	San Fernando	SFERN/PEL090	0.21

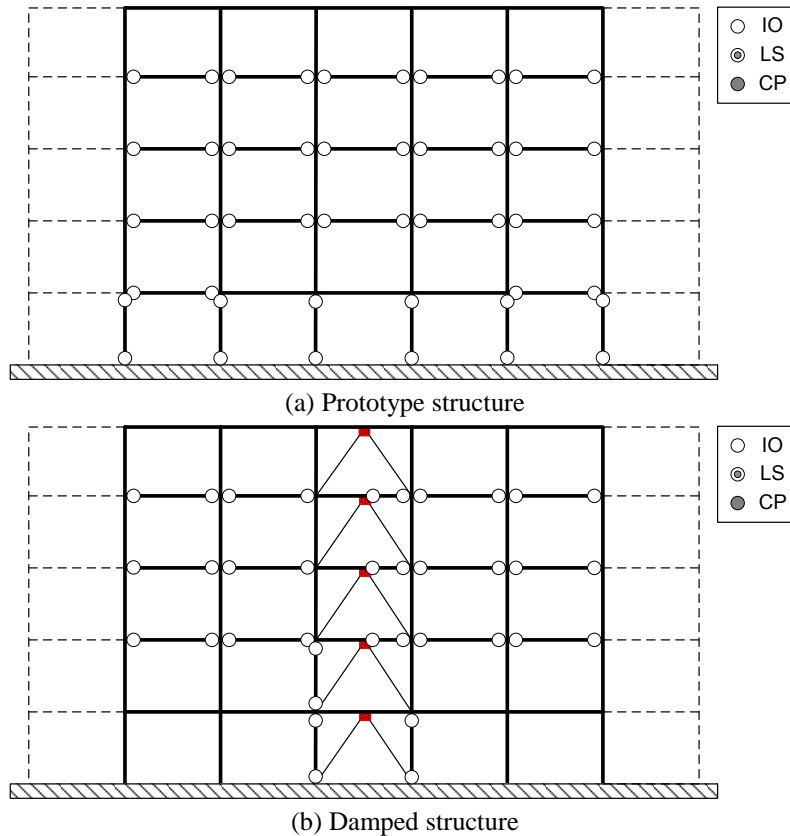


Fig. 6 Plastic hinge formation at the maximum story drift ratio of 2%

4.3 Nonlinear dynamic analysis results

Fig. 7 shows the roof displacement time histories of the prototype and the damped structures subjected to the seven ground motions presented in Table 10 which are obtained from the PEER-NGA Database. It can be observed that, even though the maximum displacements of the two systems turned out to be similar to each other, the structure with hybrid dampers experienced less permanent displacement compared with the structure without the dampers. It was observed in the analysis results that the maximum displacements of the dampers ranged from 13 mm to 20 mm under the earthquakes scaled to the MCE level. At this state of deformation, both slit and friction dampers are considered to be stable based on the observation in the previous research (Oh *et al.* 2009, DAMPTEC 2014).

Fig. 8 shows the hysteresis curve of the hybrid damper located in the first story of the model structure subjected to the Northridge earthquake (PGA=0.44 g). It can be observed that the hybrid damper shows stable hysteretic behavior under the earthquake load. Fig. 9 depicts the energy dissipation time histories in the model structures subjected to Northridge earthquake. It can be noticed that in the prototype structure about half the input seismic energy was dissipated by inelastic deformation of structural elements and the other half of the energy was dissipated by the inherent modal damping. In the structure with the dampers damage in the structural members was

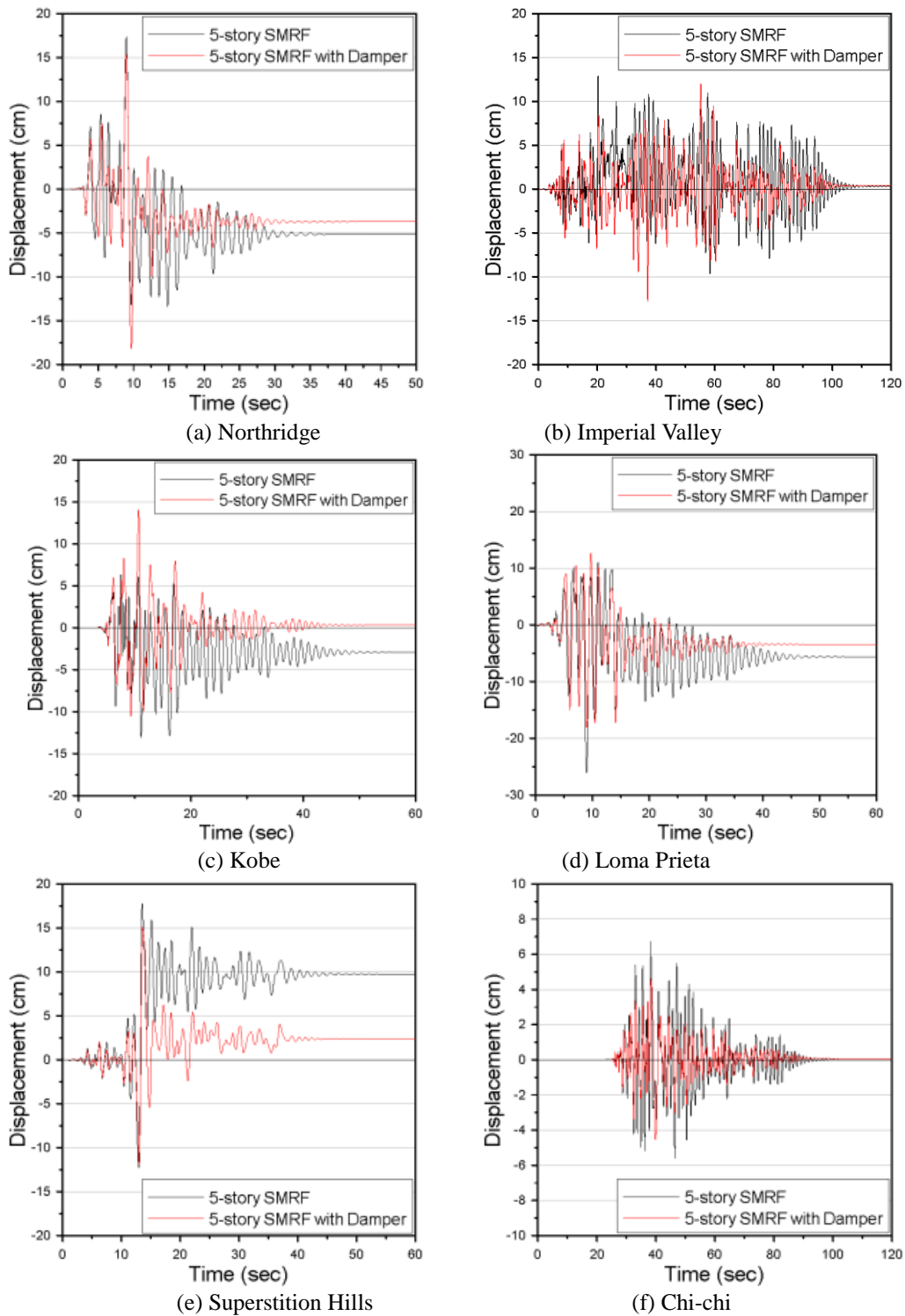
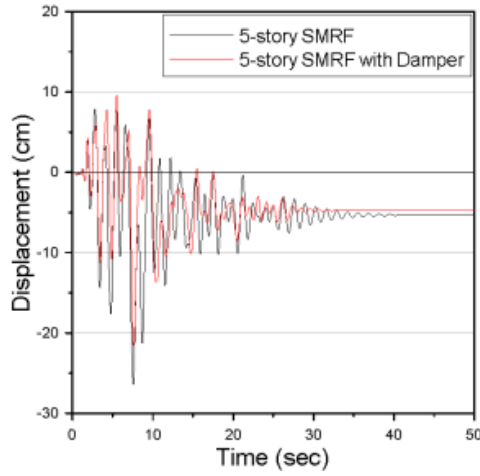


Fig. 7 Roof displacement time histories of the prototype structure and the structure with hybrid dampers subjected to the seven ground motions



(g) San Fernando
Fig. 7 Continued

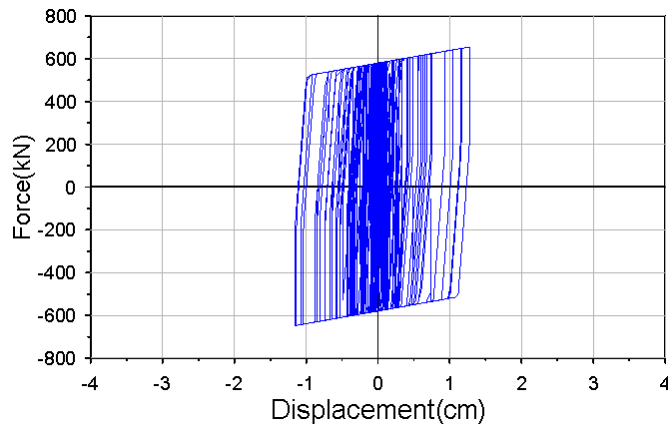


Fig. 8 Hysteresis loop of the 1st story hybrid damper subjected to Northridge earthquake (PGA=0.44 g)

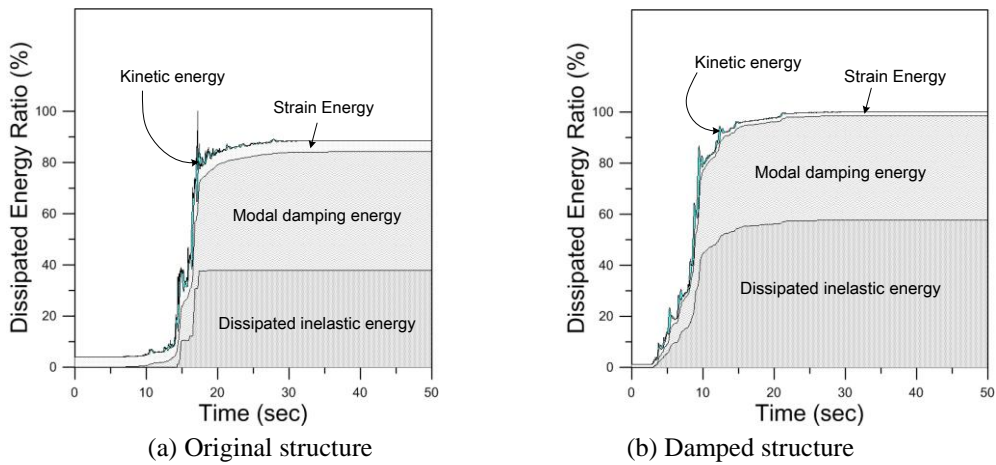


Fig. 9 Energy dissipation in the model structure subjected to Northridge earthquake

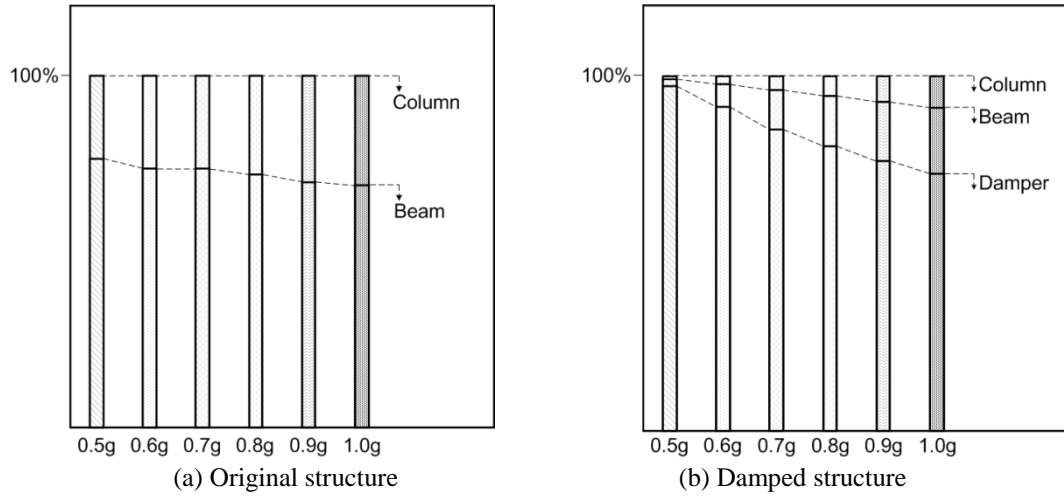
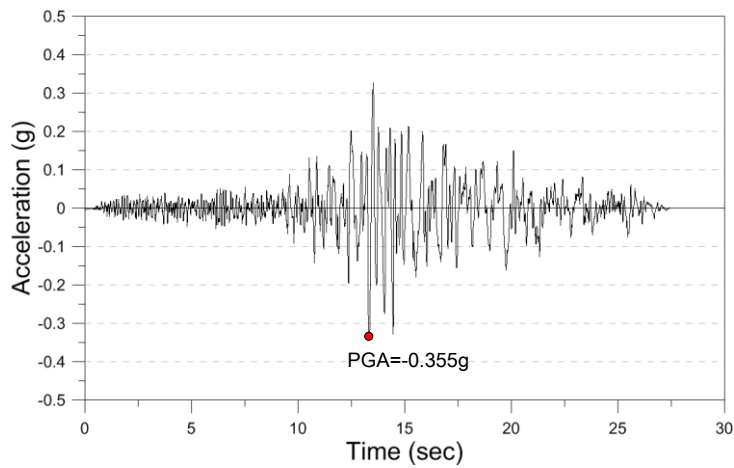
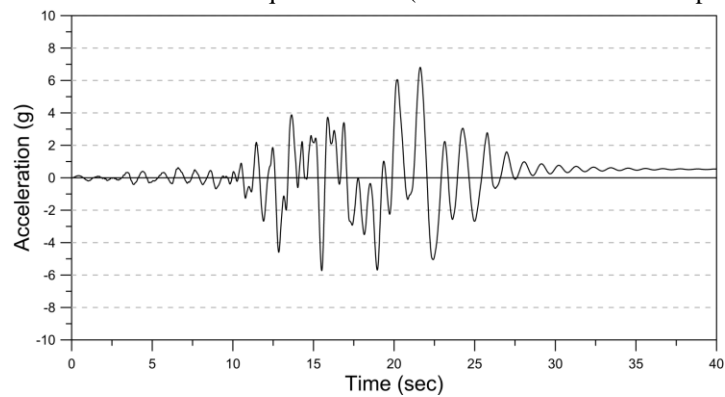


Fig. 10 Ratio of energy dissipation in the model structures subjected to Northridge earthquake with various intensities



(a) LANDERS/CLW-LN earthquake record (Record Sec. No. 848 Component 1)



(b) Roof displacement response of damped structure

Fig. 11 Ground acceleration record and the time history analysis result

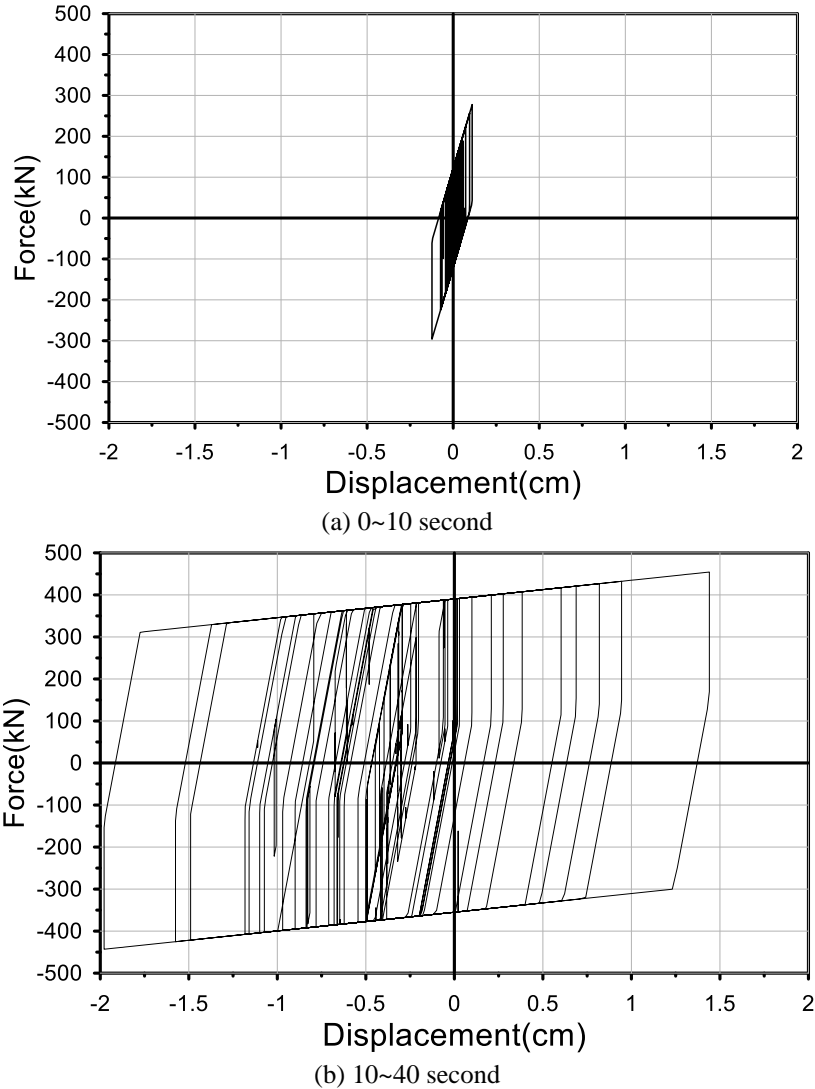


Fig. 12 Hysteresis loop of hybrid damper at the 5th story

significantly reduced compared with the damage observed in the structure designed without the dampers. The hysteretic energy dissipated by the dampers turned out to be 57% of the dissipated hysteretic energy in the system. Fig. 10 compares the dissipated energy in the model structures subjected to the Northridge earthquake with its spectral acceleration at the fundamental natural period of the model structure varied from 0.5 g to 1.0 g. No plastic hinge was observed at the spectral acceleration smaller than 0.5 g. In the damped structure it can be observed that as the spectral acceleration increases the portion of the energy dissipated by the beams and the columns gradually increases. However even at the spectral acceleration of 1.0 g the energy dissipated by the dampers exceeded 70 % of the total dissipated energy.

Fig. 11 depicts the time histories of the Landers earthquake ground acceleration and the roof

displacement response obtained from nonlinear dynamic analysis of the damped structure, where it can be observed that both the ground acceleration and the displacement response are very small up to 10 seconds and increase significantly after that time. In Fig. 12 the hysteresis curves of the hybrid damper located in the 5th story are plotted separated into two parts, which show that only the friction device yielded and the slit damper remained elastic during the first 10 seconds when the amplitude of the ground motion was small (Fig. 12(a)), and that both the slit and friction devices yielded after 10 seconds (Fig. 12(b)).

4.4 Probability of reaching a limit state

In this section the safety assessment of the model structure with hybrid slit-friction dampers was conducted based on probabilistic approach using fragility analysis. Seismic fragility is the probability that the response of a structure exceeds a limit state when subjected to a seismic event of specified intensity. In this paper fragility analyses of the model structure were carried out using 44 earthquake records provided in the PEER-NGA Database, using the spectral acceleration as the seismic intensity (*SI*) measure. The seismic fragility is described by the conditional probability that the structural capacity, *C*, fails to resist the structural demand, *D*, given the seismic intensity hazard, *SI*, and is modeled by a lognormal cumulative distribution function as follows (Celik and Ellingwood 2009)

$$P[C < D | SI = x] = 1 - \Phi \left[\frac{\ln(\hat{C} / \hat{D})}{\sqrt{\beta_{D|SI}^2 + \beta_C^2 + \beta_M^2}} \right] \quad (13)$$

where $\Phi[\cdot]$ =standard normal probability integral, \hat{C} =median structural capacity, associated with the limit state, \hat{D} =median structural demand, $\beta_{D|SI}$ =uncertainty in *D*, β_C =uncertainty in *C*, and β_M =modeling uncertainty. FEMA P695 (2009) provides β_{TOT} , the total system collapse uncertainty, for the uncertainty in the normal probability integral function Φ in Eq. (13) based on the record-to-record uncertainty, design requirements related uncertainty, test data-related uncertainty, and the modeling uncertainty. In this study the total system collapse uncertainty, β_{TOT} , provided in the FEMA P695 (2009) was used for the uncertainty in the lognormal cumulative distribution function. The design requirement related uncertainty and the test data-related uncertainty were assumed to be ‘Good’ and ‘Fair’, respectively, and the modeling uncertainty was assumed to be ‘Good’. These assumptions led to the total system collapse uncertainty equal to 0.6, which was used throughout this study.

Nonlinear incremental dynamic analyses of the prototype and the damped structures were conducted using the 22 pairs of the far field ground motions provided by the PEER NGA Database (2006) to establish the median and the standard deviation of the collapse capacity of each analysis model. Fig. 13 depicts the spectral acceleration vs. maximum inter-story drift ratio curves obtained by incremental dynamic analyses of the prototype structure (Fig. 13(a)), the damped structure with hybrid dampers (Fig. 13(b)), and the damped structure with only slit dampers (Fig. 13(c)) and only friction dampers (Fig. 13(d)) having the same strength with the hybrid dampers. Based on the incremental dynamic analysis results the probability of reaching the limit states and the corresponding fragility curves were drawn for the four different damage states defined in the HAZUS (1997), which are Slight, Moderate, Extensive, and Complete damages. The Slight

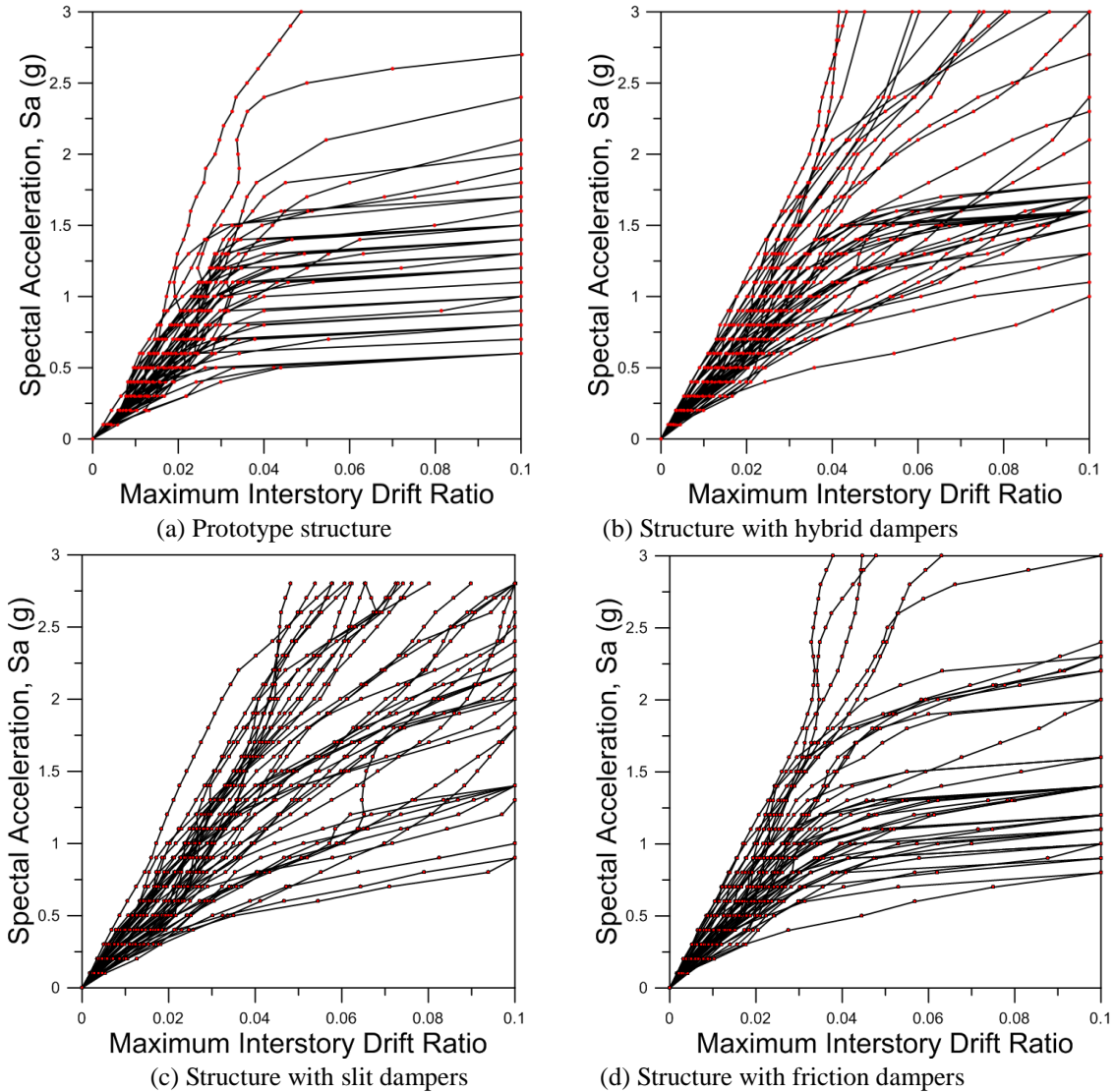


Fig. 13 Incremental dynamic analysis results of the model structure

Table 11 Damage index and corresponding inter-story drift ratio used in the fragility analysis

	Inter-story drift ratio			
	Slight	Moderate	Extensive	Complete
Prototype structure	0.0041	0.0059	0.0112	0.0271
Damped structure	0.0073	0.0099	0.0146	0.0288

damage is defined as the state with minute cracks, and the Moderate damage is the state with formation of wide spread cracks with partial yielding. In the Extensive damage state part of the structure has reached ultimate states, and in the Complete damage state the structure is near

collapse. In this study the criteria for the Slight and the Moderate damage states were defined as the inter-story drifts corresponding to 70% and 100% of the yield point, respectively, when the load-displacement relationship was idealized as bi-linear curves. The complete damage state was defined as the state at which the strength is reduced to 80% of the maximum strength. The Extensive damage was defined as the point which divides the distance between the Moderate and the Complete damage points by 1:3. The damage index and the corresponding inter-story drift ratio used in the fragility analysis are shown in Table 11. Fig. 14 depicts the fragility curves of the model structures obtained from the IDA results, where it can be observed that the probability of reaching the damage index is largest in the prototype structure which was designed using 100% of design base shear without dampers in all damage states. However the difference in the failure probability becomes smaller as the damage state changes from Slight to Complete. This implies that the damped structure designed following the ASCE 7-10 process with reduced design base shear can be effective in enhancing seismic safety against small to medium-level earthquakes. It also can be observed that, even though the difference is only minute, the failure probabilities of the structure with all-friction dampers and hybrid dampers are smallest in the Slight damage state.

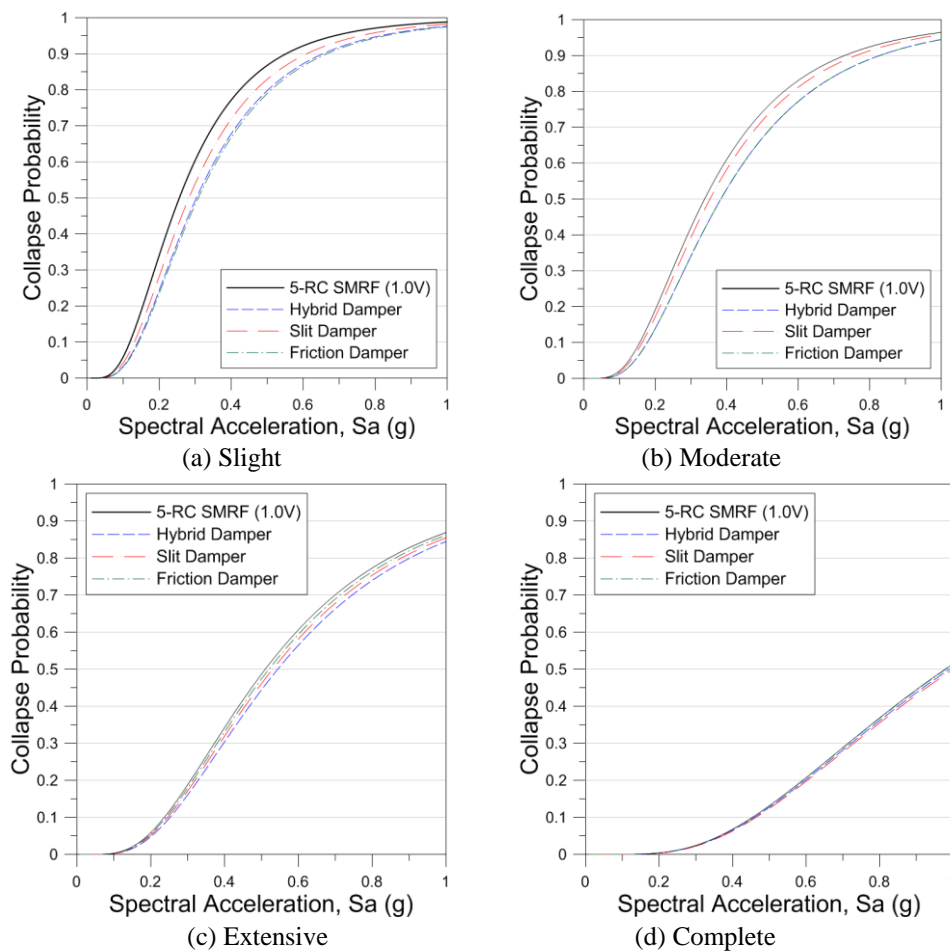


Fig. 14 Fragility curves of the model structures

However as the damage index becomes more severe to Moderate and Extensive, the failure probability becomes smallest in the structure with the hybrid dampers. In the Complete damage state the collapse probabilities of all structures are almost the same regardless of whether dampers are installed or not or which dampers are installed.

5. Conclusions

This study investigated the seismic performance of a hybrid passive energy dissipation device composed of a friction damper and a steel slit damper. The structure with dampers was designed with reduced seismic load as specified in the ASCE 7-10. The effect of the device was verified by nonlinear dynamic analysis and the probability of reaching a limit state was investigated by fragility analysis. The analysis results showed that the dissipated inelastic energy was concentrated in the hybrid dampers and the damage in structural members was greatly reduced. It was also observed that, even though the maximum displacements were similar to each other, the residual displacement was significantly reduced in the structure with hybrid dampers. The fragility analysis results showed that the dampers designed following the ASCE 7-10 process were effective in enhancing seismic safety of a structure against small to medium-level earthquakes. For large earthquakes the failure probabilities of the structures were almost the same regardless of the installation of the dampers. The structure with all-friction dampers and hybrid dampers designed to have the same overall strength turned out to have smallest fragility in the Slight damage state. However as the damage state became more severe to Moderate and Extensive states, the fragility becomes smallest in the structure with the hybrid dampers. In the Complete damage state the collapse probabilities of all structures turned out to be almost the same.

Acknowledgements

This research was supported by a grant (13AUDP-B066083-01) from Architecture & Urban Development Research Program funded by Ministry of Land, Infrastructure and Transport of Korean government.

References

- ACI Committee 318 (2011), Building Code Requirements for Structural Concrete and Commentary.
- American Society of Civil Engineers (2010), *Minimum Design Loads for Buildings and Other Structures (ASCE/SEI 7-10)*: Reston.
- Aydin, E., Boduroglu, M.H. and Guney, D. (2007), "Optimal damper distribution for seismic rehabilitation of planar building structures", *Eng. Struct.*, **29**(2), 176-185.
- Bergman, D.M. and Goel, S.C. (1987), *Evaluation of cyclic testing of steel plate devices for added damping and stiffness*, Report no. UMCE87-10. The University of Michigan.
- Blau, P. (2001), *Compositions, functions, and testing of friction brake materials and their additives*, Technical Report ORNL/TM-2001/64, Oak Ridge National Laboratory.
- Chan, R.W.K. and Albermani, F. (2008), "Experimental study of slit damper for passive energy dissipation", *Eng. Struct.*, **30**(4), 1058-1066.
- Celik, O.C. and Ellingwood, B.R. (2009), "Seismic risk assessment of gravity load designed reinforced

- concrete frames subjected to Mid-America ground motions”, *J. Struct. Eng.*, **135**(4), 414-424.
- Chen, C.-S., Chen, K.-C., Pong, W.S. and Tsai, C.S. (2002), “Parametric study for buildings with combined displacement-dependent and velocity-dependent energy dissipation devices”, *Struct. Eng. Mech.*, **14**(1), 85-98.
- Choi, H. and Kim, J. (2006), “Energy-based seismic design of buckling-restrained braced frames using hysteretic energy spectrum”, *Eng. Struct.*, **28**(2), 304-311.
- Choi, K.S. and Kim, H.J. (2014), “Strength demand of hysteretic energy dissipating devices alternative to coupling beams in high-rise buildings”, *Int. J. High-Rise Build.*, **3**(2), 107-120
- DampTech (2014), Friction Dampers-Capacities and Dimensions. <http://www.dampTech.com/download.html>
- Kim, J., Park, J. and Kim, S.D. (2009), “Seismic behavior factors of buckling-restrained braced frames”, *Struct. Eng. Mech.*, **33**(3), 261-284.
- Kim, J., Choi, H. and Min, K. (2011), “Use of rotational friction dampers to enhance seismic and progressive collapse resisting capacity of structures”, *Struct. Des. Tall Spec. Build.*, **20**(4), 515-537.
- Lee, S.K., Park, J.H., Moon, B.W., Min, K.W., Lee, S.H. and Kim, J. (2008), “Design of a bracing -friction damper system for seismic retrofitting”, *Smart Struct. Syst.*, **4**(5), 685-696.
- Marshall, J.D. and Charney, F.A. (2012), “Seismic response of steel frame structures with hybrid passive control systems”, *Earthq. Eng. Struct. Dyn.*, **41**(4), 715-733.
- Murakami, Y., Noshi, K., Fujita, K., Tsuji, M. and Takewaki, I. (2013), “Simultaneous optimal damper placement using oil, hysteretic and inertial mass dampers”, *Earthq. Struct.*, **5**(3), 261-276.
- Oh, S.H., Kim, Y.J. and Ryu, H.S. “Seismic performance of steel structures with slit dampers”, *Eng. Struct.*, **31**(9), 1997-2008.
- Patel, C.C. and Jangid, R.S. (2011), “Dynamic response of adjacent structures connected by friction dampers”, *Earthq. Struct.*, **2**(2), 149-169.
- Perform 3D (2006), Computer and Structures, Inc. PERFORM User Guide ver 4.
- Suresh, G. and Andy, R. (1991), “Planar sliding with dry friction Part 2. Dynamics of motion”, *Wear*, **20**(2), 331-352.
- Tsai, C.S., Chen, K.-C. and Chen, C.-S. (1998), “Seismic resistibility of high-rise buildings with combined velocity-dependent and velocity-independent devices”, *ASME Pressure Vessels and Piping Conference*, San Diego, CA.
- Tremblay, R., Chen, L. and Tirca, L. (2014), “Enhancing the seismic performance of multi-storey buildings with a modular tied braced frame system with added energy dissipating devices”, *Int. J. High-Rise Build.*, **3**(1), 21-33.
- Uetani, K., Tsuji, M. and Takewaki, I. (2003), “Application of optimum design method to practical building frames with viscous dampers and hysteretic dampers”, *Eng. Struct.*, **25**(5), 579-592.